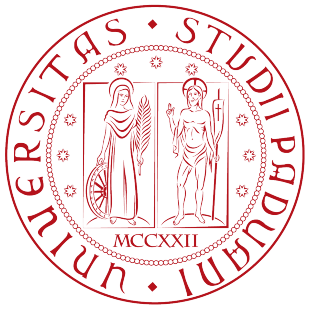

UNIVERSITÀ DEGLI STUDI DI PADOVA

Dipartimento di Fisica e Astronomia "Galileo Galilei"

Corso di Laurea in Fisica

Tesi di Laurea

Development of a new experimental setup for the measurement of electron electric dipole moment

Relatore

Prof. Giovanni Carugno

Laureando

Marcello Grenzi

Anno Accademico 2020/2021

Abstract

The progress of scientific research has led to the discovery of phenomena such as matter - antimatter asymmetry, known as the problem of baryogenesis, or the microscopic origin of dark matter, which has revealed the incompleteness of the Standard Model. Currently, it constitutes the most valid theory in order to understand most of the physical phenomena (excluding gravity), capable of predicting with absolute precision a vast quantity of events. One of the greatest fields of investigation of physics at the present time is therefore related to the attempt to find a way around the Standard Model, seeking experimental evidence that could indicate the road towards the discovery of new physics. A significant obstacle is constituted by the scale of energies required in these studies, often beyond the realms of LHC, currently the most powerful particle accelerator available to us. With recent innovations, an important contribution could therefore stem from low-energy precision measurements. In this perspective, the search for measurement of the electric dipole moment (EDM) of elementary particles, as the electron, is proposed, as a similar discovery would constitute direct proof of the violation of symmetries for time reversal (T) and parity (P) on a scale not envisaged by the Standard Model. A measurement of this kind has still not been made due to the extreme sensitivity necessary, however good progress has been made in achieving fairly high levels of precision. This thesis aims to highlight the theoretical importance of a measurement of the EDM of elementary particles with particular attention to the case of the electron, then illustrating some of the most relevant experimental approaches used. In particular, the focus will be on a non-spectroscopic technique that involves the use of polar diatomic molecules trapped in a parahydrogen matrix; in this regard, the results of a number of studies concerning portions of the experimental setup will finally be presented, performed at the INFN National Laboratories, based in Legnaro, Padua, Italy.

Contents

Introduction

The surprising and mysterious rationality that governs the behaviour of the Universe, subject of study of Physics and lively topic of discussion for the philosophy of science, is clearly evident in the symmetries that are revealed by the study of natural phenomena. The word "symmetry" refers to the invariance of a physical system that undergoes a certain transformation[1], a property that generates harmony, simplicity and "mathematical beauty", characteristic of the most important physical theories. If, naively, we might think that the concept of symmetry in physics plays an essentially "aesthetic" role, in reality its mathematical formalisation has led to extremely significant developments in the field of modern and contemporary physics, so much so that some of the greatest discoveries of theoretical physics of the XX century can be seen as discoveries of the existence of particular properties of symmetry of the physical laws.

The important role played by symmetries in physics is further evidenced by the fact that not only these but also their violations are fundamental for the understanding and interpretation of Nature. In fact, within the theories governed by a solid regularity, a symmetry breaking is a very interesting phenomenon. All this is quite relevant in the current scientific development beyond the Standard Model (SM) as it is supposed that some of the main phenomena that are still not fully explained by physical theories in fact stem from the violation of certain symmetries. Specifically, known matter - antimatter asymmetry, the result of baryogenesis, is not fully explained by the SM, but thanks to the contribution of A. Sakharov [5] in 1967, it has been understood how a number of fundamental requirements underpin this anomaly, one of which consists of the violation of the CP symmetry of charge conjugation (that is the transformation of particles into anti-particles and vice-versa) and parity, and of the single C symmetry. If on the one hand the SM permits the violation of CP, thanks to which many phenomena related to weak interaction can be explained, such as the decay of K mesons, the envisaged degree of asymmetry is however much less than that observed in the Universe. Consequently, a theory that explains this asymmetry requires an extension of the SM of elementary particles and in particular it is necessary to identify further sources of CP violation.

Before continuing in this sense, it is appropriate to point out how the violations of C, P, T (time reversal) and of the corresponding symmetries combined two by two, have all been experimentally presented in the context of the SM. The surprising fact is that this does not occur in the case of CPT symmetry, which therefore seems to be a discreet fundamental symmetry of Nature: essentially, this means that following the exchange of particles-anti-particles, inversion of the spatial coordinates and time inversion, an equally realistic universe would be obtained. This result is known by the name of CPT theorem, demonstrated in 1954 by the German physicist Gerhart Lüders, starting from the deep-seated hypotheses of locality, unity and Lorentz invariance[2]. The interesting consequence, for our purposes, is that on the basis of this theorem, a combined violation of any two symmetries that compose CPT is perfectly equivalent to the violation of the remaining symmetry. In particular the violation of CP is equal to the non-invariance for time reversal. Therefore, trying to find new sources of violation of CP, it may help to explore the phenomena that do not respect T; included in this context is the attempt at measuring the electric dipole moment of elementary particles (EDM).

[1] Strictly, symmetry in physics refers to a transformation of the system that maps observables in other observables and pure states in other pure states, preserving the average values of the observables and the structure of the algebra that describes symmetry.

[2] An experimental failing of the CPT theorem would involve a failing of one of the hypotheses that in any case are fundamental properties of any current physical model. Up until now, no violation of such symmetry has ever been observed.

Chapter 1

The EDM of elementary particles

The electric dipole moment is a vector quantity that has great importance in many physical systems. Considering any discrete distribution of electric charges q_i, even globally neutral, the potential in a point P at a significantly large distance R from the charges can be expressed as:

$$V(P) = \frac{1}{4\pi\epsilon_0}\left(\sum_{i=1}^{N}\frac{q_i}{R} + \frac{\widehat{\boldsymbol{R}}}{R^2}\cdot\boldsymbol{d} + ...\right) \quad , \qquad \boldsymbol{d} = \sum_{i=1}^{N} q_i \boldsymbol{d}_i \tag{1.0.1}$$

known as multipole expansion. In particular $\boldsymbol{d}$ is defined electric dipole moment and is a polar vector. Classic systems that possess their own dipole moment are, for example, "asymmetric" molecules such as water and ammonia, while others can acquire an electric dipole moment for polarization via an external field. Given the huge phenomenology, it is therefore necessary to clarify why only some of these systems, namely elementary particles, are so important in understanding the T and P violation.

Two different situations can therefore be considered by way of example. Let's take $\boldsymbol{d}$ as a usual dipole moment induced by an external field $\boldsymbol{E}$. In this case, by the laws of electrostatics, the dipole is proportional to the field applied, $\boldsymbol{d} = \alpha\boldsymbol{E}$, and the Hamiltonian that describes the interaction between the induced dipole and the electric field is naturally:

$$H = -\boldsymbol{d}\cdot\boldsymbol{E} = -\alpha E^2. \tag{1.0.2}$$

The Hamiltonian is clearly even and does also not undergo alterations due to time reversal as $\boldsymbol{E}$, polar vector, does not change sign (and in any case it is squared). Therefore both P and T are respected also in the presence of EDM and no contraindications with the theory arise. Now instead let's consider an elementary particle. The fundamental observation is that as a consequence of the Wigner Eckart theorem, an eventual EDM must lie along the direction of spin, that is $\boldsymbol{d} = d_{EDM}\boldsymbol{S}$. Therefore if a non-null EDM exists, so the Hamiltonian of interaction with an external field E will clearly be:

$$H = -d_{EDM}\boldsymbol{S}\cdot\boldsymbol{E} \tag{1.0.3}$$

that however is no longer P invariant as $\boldsymbol{E}$, which is a polar vector, changes sign while $\boldsymbol{S}$, which is an axial vector, remains unchanged. Furthermore, this Hamiltonian is not even T invariant, as exactly the same opposite condition occurs, that is $\boldsymbol{E}$ does not change sign while $\boldsymbol{S}$ does. Therefore in this case, the existence of an EDM other than zero leads to the violation of such symmetries. More precisely, by itself this might not be a problem because, as stated in the introduction, the SM involves sources of CP violation (and therefore T) to explain phenomena linked to the weak interaction, therefore the existence of a non-null EDM would be permitted without contradictions. However, the complication lies in the fact that the issue always concerns very weak violations, which lead to an important suppression of the EDM of particles of many orders of magnitude [18]. For example, for the electron, reference is made to values that are less than $10^{-38}\, e\, cm$ or, according to other more recent studies, even below $10^{-44}\, e\, cm$ (Pospelov and Ritz, 2014), in any case at least 9/10 orders of magnitude below

the current experimental limit. Conversely, various theories beyond standard model (BSM), first and foremost Supersymmetry, admit to the existence of EDM of elementary particles with much higher values, comparable to the orders of magnitude that are currently accessible experimentally.

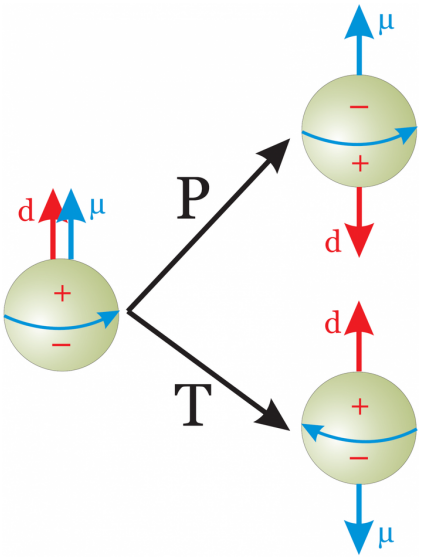

Figure 1.1: Effect of T and P symmetries on EDM d and MDM μ of an elementary particle.

It is therefore clear that a measurement of the EDM on similar scales would not only be a demonstration of the violation of T that is markedly beyond the previsions of the SM but would also be an important test of consistency of BSM theories. This produces an even greater interest in taking precision measurements for the observation of EDM, an objective that has not yet been achieved. Starting from 1950 with the first experiments of Ramsey and Purcell on neutrons, research has continued to intensify, developing numerous innovative theories and reaching ever higher precisions. The results achieved up until now will be presented below, then focussing attention on the experimental approaches used in the case of the electron EDM (eEDM), which will be the true protagonist of the laboratory analysis.

Chapter 2

Experimental approaches to the EDM

2.1 Overview of the various physical systems

Before starting the discussion, it is worth giving an idea of just how complex these measurements are. Considering, for example, the case of the electron, the best current limit of the EDM (paragraph 2.2.1) is $d_e < 1.1 \cdot 10^{-29}\ e\,cm \sim 10^{-48}\,C\,cm$ obtained with electric fields of the order of $E = 100\,GV/cm$. This is equivalent to an energy of $\epsilon = d_e\,E \sim 10^{-37}\,J = 10^{-18}\,eV$, in other words no less than 13 orders of magnitude less than the already small normal Zeeman effect with $B = 1\,T$.

The techniques used to measure the EDM fall within the huge category of "atomic, molecular and optical physics techniques" (AMO) and vary significantly depending on the type of particle being studied. Recent progress in this sector have led to the use of such techniques in numerous areas of physics, which range from research for dark matter to general relativity. With regard to the study of EDM, despite the high number of case studies, a number of methods can be distinguished based on the system being studied: neutrons, atom and molecule systems (paramagnetic, diamagnetic, polar), or single charged particles. Generally, most experiments are based on the observation of how external electric and magnetic fields ($\boldsymbol{E}$, $\boldsymbol{B}$) interact respectively on EDM and MDM, which are directly correlated to the spin. The system will therefore generally be described by the following Hamiltonian:

$$H = -\boldsymbol{\mu} \cdot \boldsymbol{B} - \boldsymbol{d} \cdot \boldsymbol{E} \tag{2.1.1}$$

Research into EDM is often reduced to measuring the precession frequency of the spin around the direction of the fields $\boldsymbol{E}$ e $\boldsymbol{B}$, known as Lamor frequency, studying possible variations of such frequency under parity (inversion of fields). Starting from these basic considerations, the measurement techniques vary substantially depending on the characteristics of the system being analysed. Neutrons were the first to be studied, starting from 1950 (Ramsey and Purcell), as they do not present electric charge, a fact which makes them easier to measure given that the application of electric fields doesn't cause them to move. The current lower limit for the EDM of the neutron is $d_n < 1.8 \cdot 10^{-26}\ e\ cm$ (90 C.L.), obtained at the Paul Scherrer Institute of Zurich via the use of ultra-cold neutrons (UCN) [7]. The higher limit of these experiments lies in the necessary intensity of the electric field which often borders on the limit of today's possibilities.

To detect the EDM of charged particles, it is necessary to use more appropriate methodologies. In particular, one of the most popular techniques employed involves the use of storage rings, that is high vacuum chambers with a generally toroidal configuration in which the accelerated particles remain in circulation for possibly quite long periods. The charged particles most studied using these techniques include the muon, the deuteron and the proton. The fundamental idea, already proposed by Shapiro [8] is based on techniques that are similar to those adopted to measure the anomalous magnetic moment of the used particles, that is, in the case of the muon for example, the difference between Dirac g-factor (g = 2) and the one experimentally measured, the so-called g-2. Thanks to

these techniques, it has been possible to obtain the best current estimate of the EDM of the muon by using precession measurements of the spin performed at the Brookhaven National Laboratory [9]: $|d_\mu| < 1.8 \cdot 10^{-19}\ e\,cm$. The Muon g-2 experiment at the Fermilab in Chicago is seeking to increase the current limit by another two orders of magnitude.

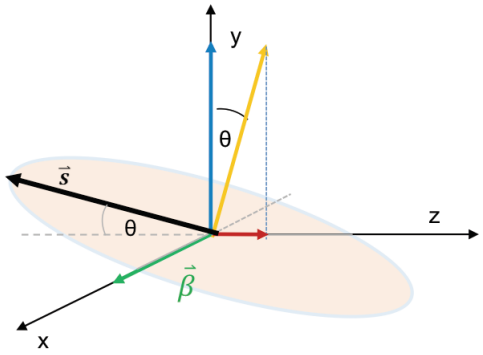

Figure 2.1: Besides the magnetic field B (in blue), a component E' also appears (in red) which causes an inclination of the precession plane of a measurable angle θ. In green the speed of the particle.

Finally, it is also possible to study the EDM using more complex apparatus, such as atoms and molecules, as their EDM could have contributions stemming from a possible EMD at subatomic level (nucleus, electrons, etc.). In particular, a permanent EDM in paramagnetic atoms derives essentially from the EDM of the electron; unlike a permanent EDM for diamagnetic systems, it is a manifestation of the so-called "Shiff moment" of the nucleus, which in turn is triggered by the difference between the distributions of the nuclear charge and the EDM of the nucleons [2]. The interest generated by these atomic and molecular systems is fuelled by some of their favourable characteristics, which, experimentally, make them easier to work with. In particular, as previously highlighted, one of the greatest difficulties in measuring the EDM of charged particles relates to the motion caused by the interaction between electric field and the particle itself. Techniques were therefore sought to balance the electric field without however cancelling the effect of a possible EDM. This allows understanding of the usefulness of an atomic system, in which electrons and nucleus, thanks to the reciprocal shielding effect, are able to resist an overall null electric field and are therefore not subject to acceleration. Various studies have been performed on diamagnetic atoms, in particular on the fundamental states of the isotopes ^{199}Hg and ^{129}Xe. Precisely, he experiement performed on the ^{199}Hg at the University of Washington in Seattle redefined the lower limit never before reached for the EDM of diamagnetic systems, $d_{Hg} < 7.4 \cdot 10^{-30}\ e\,cm$ [11].

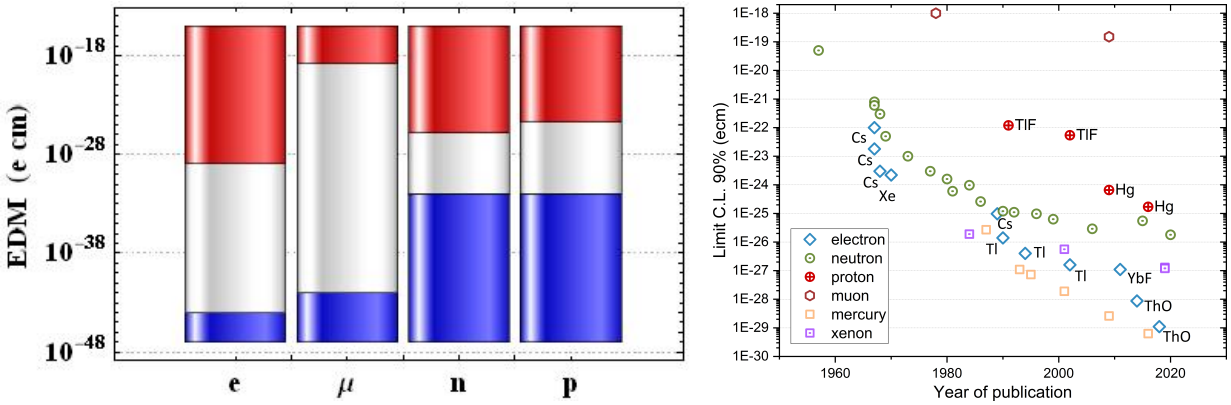

Figure 2.2: To the left in blue are show the previsions of the SM per the EDM of a number of elementary particles and in red the actual experimental limits. To the right, a chronological representation of the EDM measurements for various systems. In the case of the electron, the method used is also highlighted.

With regard to the electron, which is the particle that, from this point forward, will be focused on, the most studied systems are instead paramagnetic atoms, which possess an overall non-null electronic spin, and in particular in the last few years, a number of polar molecules that possess unique characteristics which are very favourable in terms of measuring the EDM (chap.3). A few measuring techniques used for the EDM of the electron will be illustrated below, examining in particular the experiments that, historically, have led to significant improvements in measuring sensitivity. As such, the experiment involving the ACME collaboration with the use of ThO will be addressed, which still constitutes the lower limit ever reached for the eEDM. Finally, the experiment that is currently being designed will be presented, which involves the use of BaF^+ ions trapped in a solid gas matrix, in relation to which a number of laboratory studies will then be discussed.

2.2 Electron EDM

The advantages of using atomic and molecular systems were not immediately understood as it was thought that for atoms and molecules the presence of the EDM would require a "violation" of the Schiff theorem [10]: in a system constituted by non-relativistic point particles in equilibrium under the action of electrical forces, the overall EDM is null even if the individual components present non-null EDM. In the presence of external electric field, there would also be a rearrangement of the nucleons and of the atomic electrons such that, due to the effect of shielding, the electric field perceived by each charged particle would overall be null also, however, cancelling the total EDM and thus eliminating any possibility of measurement. The first experiments thus sought to follow other roads such as the technique of measuring in storage rings, which then became the norm in experiments on the muon and improving the upper limit of the EDM by no less than 3 orders of magnitude. The true turning point however took place just a few years later.

The first experiment based on paramagnetic atoms was performed when, thanks to the work of Edwin Salpeter and Sandars [12], it was understood that the effect of shielding by electronic clouds of the atom could be partially limited due to the relativistic behaviour of the electronics, especially close to the nuclei of atoms with high Z, which generates a significant contraction of the lengths in the electron frame (remember that the Schiff theorem is not relativistic). Thanks to this aspect, for particularly large atoms, an increase of estimated atomic EDM of the order of $R = \frac{d_a}{d_e} \approx 10Z^3\alpha^2$, α fine-structure constant is even observed, which grows quickly with the atomic number Z.

atom	Z	gain factor R
Rb	27	24
Xe	54	120
Cs	55	114
Tl	81	-585

Table 2.1: Gain factors for some paramagnetic atoms used in the experiments (taken from table 6.1 [15])

In particular, in 1990 the experiment performed a Berkeley with thallium atoms (which presents a gain factor that is at least 5 times greater than all the other atoms considered) resulted in determining the best limit of the eEDM for a long period of time.

2.2.1 ACME II Collaboration ThO experiment

One of the higher limits in the use of atomic beams relates to the intensity of the electric field required to take increasingly precise measures, often not reachable by current instrumental apparatus. The use of polar diatomic molecules allows a huge reduction of this problem thanks to the presence of the strong intramolecular electric field E_{int} which affect electronics, which is often of the order of tens of

GV/cm, in other words much more powerful than the fields that can be obtained in the laboratory which normally do not exceed tens of kV/cm. Therefore, applying an external electric field E_{ext} to polarize the molecules, it will be possible to obtain overall a very powerful effective electric field E_{eff} given by the sum of contributions outside and inside the molecule, whereby the energy of interaction between E_{eff} and the possible EDM will therefore be very amplified with significant advantages in terms of measurements. The first experiment based on polar molecules which allowed lowering of the upper limit of the eEDM involved the use of a YbF beam [16]. However, this limit was improved on by no less than two orders of magnitude thanks to more recent experiments performed on ThO molecules, which in fact present an internal field that is quite markedly more intense. Furthermore, a number of experimental devices resulted in, to the extent possible, overcoming some of the major problems linked to the experiments on the beams of atoms/molecules, that is the count rate and the number of molecules available in the measurement, thereby significantly improving the statistics. Therefore, let's turn our attention to the experiment performed in 2018 [14] as an example of this category of experimental techniques, which currently determines the best limit of the eEDM.

Since 2014, the ACME collaboration, which brings together prestigious research centres from around the word, has focused its own attention on the ThO molecule which, presenting an internal field of $78\,GV/cm$ is ideally suited to eEDM measurement experiments. The most recent of these (ACME II) focuses on the sublevels $J = 1$, $M = \pm 1$ of the state $H^3\Delta_1$ of the ThO, where J is the total angular momentum and M its projection along the molecule axis. Within the external electric field $\boldsymbol{E} = E_z\hat{\boldsymbol{z}}$ along z, these states polarize this direction such that the intramolecular axis $\hat{\boldsymbol{n}}$ which points from the O to the Th is parallel or antiparallel to $\boldsymbol{E}$. To describe the orientation of the molecule, a "quantic number" $\tilde{N} = segn(\boldsymbol{E} \cdot \hat{\boldsymbol{n}}) = \pm 1$ is introduced. As is known, the application of electromagnetic fields generates splitting of the energy levels; in this experiment there are essentially 3 contributions:

- the external electric field E induces Stark effect in the levels with $M = \pm 1$, therefore causing a splitting equal to $2\,\boldsymbol{D} \cdot \boldsymbol{E}$;
- the presence of a further direct magnetic field along z, $\boldsymbol{B} = B_z\hat{\boldsymbol{z}}$, also contributes, due to the Zeeman effect, to splitting of the energy into levels with $M = \pm 1$;
- the combination between $\boldsymbol{E}$ and internal field generates an effective field $\boldsymbol{E}_{eff}$ which direction coincides clearly with z and acts directly on the eventual eEDM, causing in this case a further shift of the levels equal to $U = -\,\boldsymbol{d}_e \cdot \boldsymbol{E}_{eff}$ which should be added to the previous ones.

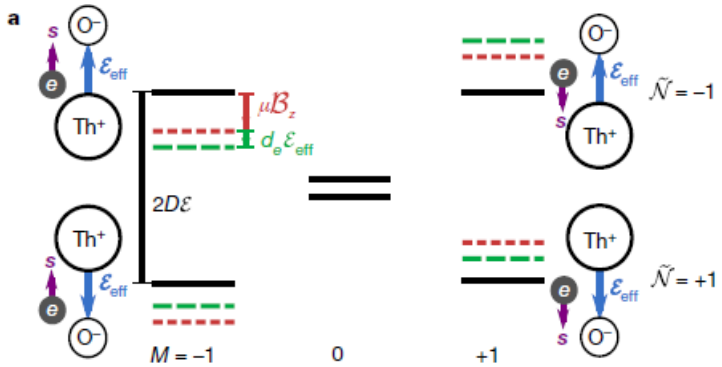

Figure 2.3: A diagram of the shift of energy levels caused by the application of external electric and magnetic fields.

The spin s of the electron lies along the spin S of the molecule and depending on whether s is parallel or antiparallel to the field $\boldsymbol{E}_{eff}$ there is a variation in the third contribution to the split in energy, depending on whether $M = \pm 1$, and it is precisely this phenomenon that is used to investigate the presence of electronic EDM. A beam of ThO radicals is therefore created, all aligned in the direction x (Figure 2.5) with coherent superposition of states $M = \pm 1$. Then the action of the electric $\boldsymbol{E}$ and

magnetic $\boldsymbol{B}$ field exercises a torque on the electric and magnetic dipoles, triggering a precession of the molecule on the xy: the molecules therefore travel for a certain length L until they meet a laser which excites them at a clearly defined frequency. The next de-excitation produces a fluorescence signal that is dependent on the angle ϕ formed by S and the polarisation of the laser. Writing the precession frequency of the spin as the definition $\omega = \frac{\phi}{\tau}$, the value of d_e is given by the following expression, where $\omega^{\widetilde{N}\widetilde{E}}$ indicates the dependance of ω on the orientation of E_{eff} in the laboratory frame, that is by the product $\widetilde{N}\widetilde{E}$:

$$d_e = -\frac{\hbar\omega^{\widetilde{N}\widetilde{E}}}{E_{eff}} \tag{2.2.1}$$

The experimental setup used to take this measurement will now be described. The ThO molecules are produced in a source consisting of a criogenic "buffer" gas in which the solid matrix of ThO_2 undergoes ablation by a laser, thus generating free ThO molecules. Thanks to the impacts with the inert buffer gas in the chamber, the molecules are cooled to $4\,K$, to then exit the chamber as a fold and intense beam, mainly in the fundamental states $|X, J = 0, 2\rangle$. Now the procedure involves creating a coherent superposition of states $M = \pm 1$. For this purpose, the beam is first cleaned of the rotational state $J = 2$, thereby allowing an increase by a factor of 2.5 of the molecule population in the state $J = 0$. This process is performed in two steps: first, the beam is stimulated for 5/7 times by laser beams (each of them is perpendiculary polarized compared to the previous one) resonant with the $|X, J = 2\rangle \longrightarrow |C, J = 1\rangle$ transition; then the final state decays for de-excitation to the fundamental one, $|X, J = 0\rangle$. Secondly, the beam of ThO enters a region with ad electric field of $100\,V/m$ where is enlightened by microwaves, in order to improve further the selection of rotational states.

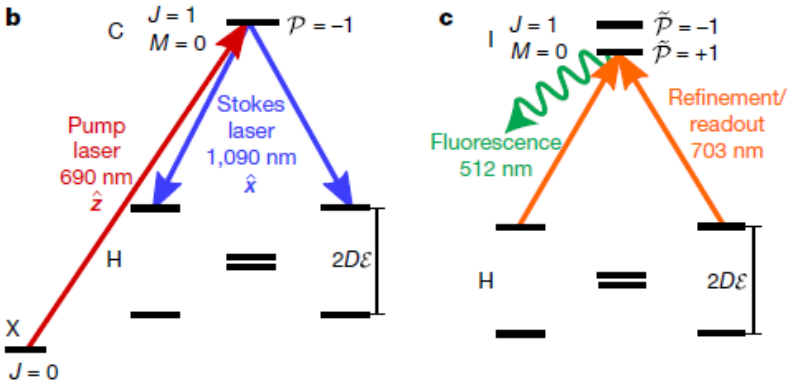

Figure 2.4: A diagram of the transitions induced by the lasers used to prepare the initial state (to the left) and for measurement/refinement (to the right).

The beam then enters a region in which a uniform electric field E_z and a magnetic field B_z are present, parallel to each other, the first generated by a pair of parallel plates, the second by coils carrying a current I. In this area, the beam undergoes a transition stimulated by two Raman pulses (STIRAP), a methodology that is widely used to transfer populations of molecules into various quantic states. STIRAP involves the use of two lasers arranged vertically along y and directed downwards, represented in red and blue in the figure 2.4. Their combined action is used to transfer the molecule from the fundamental initial state to the excited level $|H, J = 1, M = \pm 1\rangle$ intended to be studied[1]. Any imperfections that could cause systematic errors are eliminated by a $703\,nm$ refinement laser (in orange in figure 2.4) thanks to which the spin S is optimally aligned along x.

[1]This process is defined Raman scattering, in other words an anelastic scattering in which a molecule undergoes an initial stimulated excitation and a consequent de-excitation, this also stimulated from the outside, reaching, at the end, a vibrational state that is different from the initial one with the consequent emission of photons with energy different from that of the incident photons. In particular, a situation of Raman-Stokes scattering occurs if the photons emitted are less energetic than the former (therefore the end state is more excited); conversely, the event would be referred to as Raman-Anti Stokes scattering.

After this latter refinement operation, the beam possesses a coherent superposition of metastable states $|H, J = 1, M = \pm 1\rangle$ (lifetime $2\,ms$) ready to be studied.

The molecules now travel in the constant E_z, B_z fields for a distance L of approximately $20\,cm$ while the spin $\boldsymbol{S}$ precedes in the xy plane, and finally reach a laser that is identical to the readout one but with variable polarization $\hat{\epsilon}$. In particular the polarization between the directions $\widehat{\boldsymbol{X}}$ and $\widehat{\boldsymbol{Y}}$ defined in figure 2.5 is varied, with a rate of $5\,\mu s$ µs such that each molecule can be addressed by both polarizations. As shown in figure 2.4, the action of the laser produces an excited state that quickly decays, emitting a fluoresence signal at $521\,nm$, the intensity of which depends on the angle between $\hat{\boldsymbol{\epsilon}}$ and $\boldsymbol{S}$ and is acquired by 4 pairs of photomultipliers. The following asymmetry is then calculated:

$$A = \frac{S_X - S_Y}{S_X + S_Y} \propto cos(\phi) \tag{2.2.2}$$

which contains the information on ϕ from which, as seen in (2.2.1), it is possible to infer an estimate of d_e, which after 2 months of measurements is equal to $d_e = (4.3 \pm 3.1_{stat} \pm 2.6_{syst}) \cdot 10^{-30}\ e\,cm$ which is equivalent to the upper limit of $d_e < 1.1 \cdot 10^{-29}\ e\,cm$, improving of 1 order of magnitude the previous limit. The main sources of systematic errors are found in the small gradients present in the electric and magnetic fields that are not exactly constant along z: this causes a different precession of the spin depending on the coordinate z of the molecule inside the beam.

The improvement with respect to the previous experiments is in any case significant. First and foremost, the polarity inversion rate of the readout laser is much less than the time scales of the fluctuations in the number of molecules in the beam and consequently the asymmetry term A is almost independent from them. Furthermore, the technique of producing the beam of molecules in the criogenic source has enabled a significant raising of the number of molecules available compared with the previous experiments, even though this statistical problem still constitutes a limit in these types of measurements. The next experiments of this type involve the production of ThO through the reaction $Th + ThO_2 \rightarrow 2ThO$ instead of laser ablation, guaranteeing a greater gain in terms of beam molecular density. Furthermore, the use of STIRAP for preparation of the initial state, combined with the shorter wavelength of the light emitted at the end ($512\,nm$, for which the photomultipliers have a greater efficiency with respect to the $690\,nm$ of ACME I) has increased the efficiency of the detection rate of a 400 factor compared to past experiments. Finally it is pointed out that, unlike the ^{205}Tl experiment for example, it is possible to explore the shift of energy between the two possible orientations of the EDM with respect to the spin without necessarily having to reverse the external electric field, thus eliminating any systematic errors linked to this procedure.

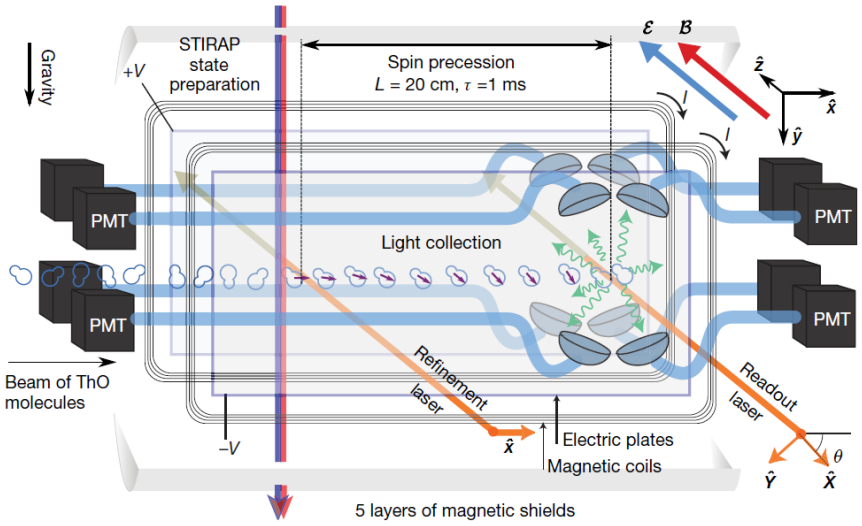

Figure 2.5: A scheme of the experimental apparatus used

Chapter 3

A new proposal for measurement of the eEDM

3.1 Theoretical description

Currently, the most promising studies for EDM research of the electron are being focused on techniques that continue to involve the use of polar molecules, seeking to exceed the limitations determined in past experiments based on atoms/molecules beams which, as seen, are linked, above all, to statistics (number of molecules, the counting rate, etc.). One theoretical proposal is contained in [17], in which a non-spectroscopic technique is discussed which involves trapping reactive, diatomic molecules in a cold solid matrix, such as a noble gas crystal. This combination seems to be able to significantly improve the sensitivity of experiments at least 1 order of magnitude below the present limit. In particular, attention is being turned to molecular radicals that possess a free electron. A set of radicals in thermodynamic equilibrium all the temperature T is thus considered; keeping in mind that the EDM lies along the direction of the spin, thanks to the coupling between eEDM and E_{int} of the molecule, an average magnetic moment (which violates CP) for each molecule is obtained, equal to:

$$\left\langle \mu^{CP} \right\rangle \sim \frac{\mu_B \, d_e \, E_{eff}}{k_B T} \tag{3.1.1}$$

where d_e is the eEDM, E_{eff} the internal electric field, T the temperature of the system. For biatomic radicals, this magnetic moment lies along the axis of the molecule. Remember [12] that E_{eff} in the formula is proportional to Z^3, with Z atomic number of the heaviest atom of the radical. Therefore, to optimise the parameters of the experiment, it is worthwhile considering heavy radicals, such as BaF, YbF, HgF and other mercury derivatives.

molecule	$\boldsymbol{E_{eff}}$ **(GV/cm)**	$\boldsymbol{D}$	$\boldsymbol{\langle n_z \rangle}$	**Ref.**
YbF	23	3.91	-	
HgF	115	2.92	-	19
HgCl	114	2.96	-	19
HgBr	109	2.71	0.11	19
HgI	109	2.06	0.08	19
BaF	8	3.17	0.13	

Table 3.1: Some values of relevant parameters of interesting molecules

If for a causal set of radicals the magnetisation would be on average null, applying an external direct electric field $\boldsymbol{E}$ along z it would be possible to polarize the molecules thanks to their classic electric dipole moment $\boldsymbol{D}$, thus obtaining a new magnetic moment equal to:

$$\left\langle \mu_{mol}^{CP} \right\rangle \sim \frac{\mu_B \, d_e \, E_{eff}}{k_B T} \times \langle n_z \rangle \tag{3.1.2}$$

where $\langle n_z \rangle$ is the average projection of the molecular axis onto the $\boldsymbol{E}$ field. In this way, it is possible to produce a non-null magnetisation of the set of radicals, obtaining a very weak magnetic field B^{CP}, proportional to the EDM, which it is possible to measure:

$$B^{CP} = \mu_0 \gamma n_M \left\langle \mu_{mol}^{CP} \right\rangle \tag{3.1.3}$$

where n_M is the density of the molecule number and γ is a geometric factor. From the measurement of this magnetic field, it is therefore possible to obtain information on the EDM of the electron. Given that B^{CP} is generally quite weak (see 3.1.7), besides appropriately choosing a radical with high E_{eff} it is advisable to take further actions to optimise the measurement. First and foremost, it is necessary to maximise the density n_M of the molecules and to reduce the temperature in such a way as to increase the magnetic field produced, as well as limiting the problem of the low statistics highlighted in previous experiments. However, radicals are very chemically reactive, which makes it difficult to get close to them. The radicals are thus trapped in a particularly cold matrix (a few Kelvin) measuring just a few mm in height and approximately $1\,cm^2$, wide, and within it the individual molecules act as if there were quasi-free, without interacting to a large extent with each other.

There is in any case an upper limit for the density of the molecules such that they can be considered non-interacting, which can be found but requiring that their thermal agitation is greater than the dipole-dipole interaction between them. By parameterising the thermal energy with $K_B\,T$ and the interaction with the dipole moment $\boldsymbol{D}$ of the molecule, this maximum density can be estimated as:

$$n_{max} \sim \frac{3}{4\pi} \frac{k_B T}{D^2} \tag{3.1.4}$$

For $D = 1\,Debye$, $T = 4K$, we obtain $n_{max} \sim 1.3 \cdot 10^{20}\,cm^{-3}$. The types of matrix that we consider (Ar, Ne, p-H2, ...) present density values of about $2.3 \cdot 10^{22}\,cm^{-3}$ corresponding to a lattice parameter of $3.5\,A$, so it could be possible to obtain a density ratio between radicals and matrix of about 1:200. A fundamental condition for running of the experiment is that the molecules, despite being trapped, are in any case free to rotate within the matrix and in fact, the only way to module B^{CP} is act on n_z, that is on the orientation of the molecules. With this trick, the application of a variable external electric field is able to produce a magnetic field B^{CP} in turn variable and thus more easily identifiable.

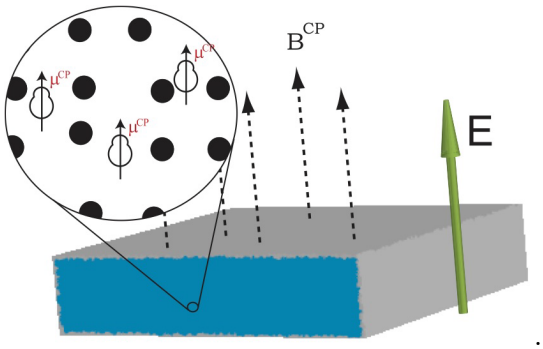

Figure 3.1: Diagram of the gas matrix with the trapped radicals

The choice of the matrix to be used is therefore of fundamental importance, compatibly with the dimensions of the trapped radicals. The matrix contains an approximately periodic potential V consisting of wells in which the molecules are found. The ideal situation is created when an alignment of the molecules is guaranteed without preventing its rotation (alignment does not mean orientation, the molecules can be aligned in the wells without necessarily being oriented in the same direction).

Firstly, it is advisable to use matrices with shallow potential wells, as in the case, for example, in the parahydrogen p-H2. The role of the matrix therefore becomes simply that of bearing structure to stop the linear movement of the molecules. Furthermore, to guarantee alignment, the rotational kinetic energy of the molecule must be sufficiently low; this is possible by exploiting molecules with a high moment of inertia, such as BaF, remembering that: $E_{rot} = \hbar^2 J(J+1)/2I$.

Besides these measures, the fundamental parameter to regulate the value of the magnetic field B^{CP} is n_z. As shown in [17], the value of n_z naturally tends to 1 in the limit of strong electric fields, while for weak fields, the intensity is given by:

$$\langle n_z \rangle \sim \frac{D\widetilde{E}}{k_B T} \left\langle n_z^2 \right\rangle \tag{3.1.5}$$

with $\widetilde{E} = \frac{E}{\epsilon}$ (microscopic electric field, ϵ dielectric constant of the medium). ϵ it is approximately 1 for the matrices considered, comparable to the vacuum, to which, however, should be added the contribution given by the molecules trapped, obtaining:

$$\epsilon \sim 1 + 4\pi n\alpha \sim 1 + \frac{4\pi}{3} n \frac{D^2}{k_B T} \tag{3.1.6}$$

with α polarisability of the molecule. Therefore, as n_z^2 is approximately $1/3$ for isotropic crystalline systems as the matrices used, considering the condition of maximum density n_{max} and external field values of $10\,kV/cm$, the polarization values are calculated in table 3.1. The BaF appears to be the radical with the most convenient value of n_z. Clearly as the intensity of the magnetic field $\boldsymbol{E}$ increases, higher values of n_z can be obtained. Using BaF parameters in table 3.1, for a matrix measuring $0.4mm$ and area $1\,cm^2$, n_M as in (3.1.4), we obtain an extremely small field:

$$B^{CP} \sim 1.8 \cdot 10^{-21}\, T \qquad (\ \gamma = 0.4,\ \ T = 4K,\ \ n_M = 1.3 \cdot 10^{20} cm^{-3},\ \ d_e \sim 10^{-30} e\, cm\ ) \tag{3.1.7}$$

One possibility could be measuring it with a SQUID, but this idea still needs to be tested. In conclusion, is convenient to use of diatomic molecules with high dipole-electric moment $\boldsymbol{D}$, with high moment of inertia I, in a matrix of p-H2 with a possibly very intense external field $\boldsymbol{E}$.

3.2 Experimental setup

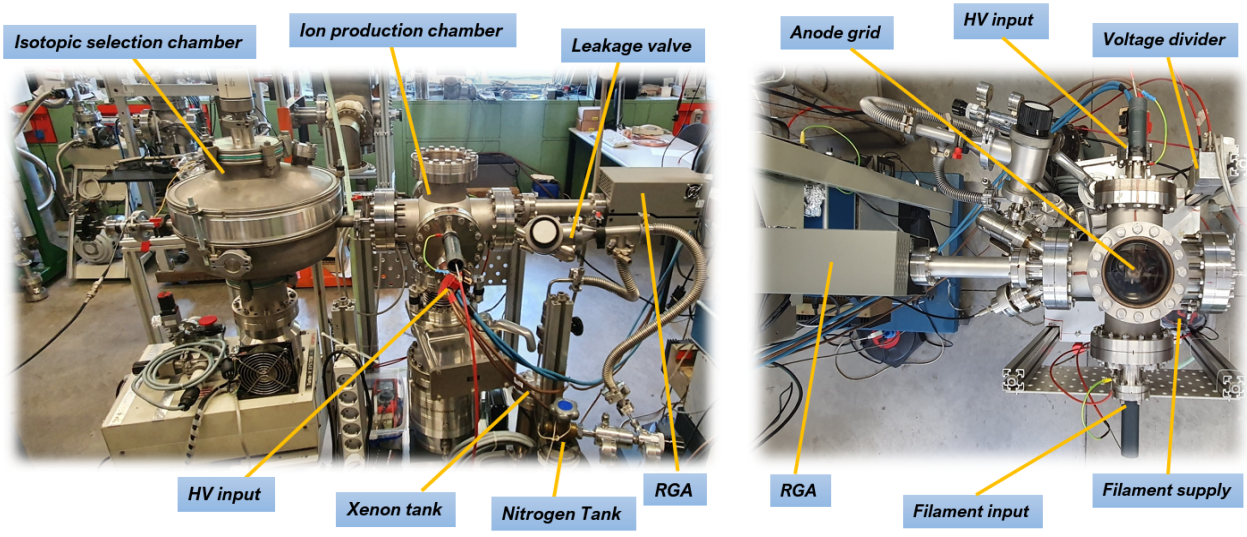

Figure 3.2: To the left a complete image of the experimental set-up. To the right, a top view image of the production chamber.

The apparatus designed for these new types of experiment on the eEDM is divided into 4 main stages: **(1)** production of ion molecular beam, **(2)** isotopic selection, **(3)** neutralization of the ions and **(4)** mixing in the parahydrogen matrix. The analysis contained in this thesis work focuses only on the first two stages, while the measurements were only taken for the first, that is currently the only in operation. Given its advantageous properties, it was decided to work with BaF_2 (which produce BaF^+ due to ionization), which comes in the form of small colourless crystals.

3.2.1 Production of ion molecular beam

The production environment consists of a high-vacuum chamber ($10^{-6}/10^{-7} mbar$) equipped with a turbine with pumping speed of $700\, lt/s$. It is important to determine the composition of the various atomic and molecular species of the chamber in order to be able to highlight all the possible sources of noise and to monitor the production of the BaF_2. For this purpose, a Residual Gas Analyzer (RGA) of the Stanford Research Systems is used, that is able to measure the partial pressure of the various components present on a $200\, amu$ (atomic mass units) range.

Within the chamber there is a small tungsten crucible covered in ceramic material, containing powdered BaF_2. Tungsten, thanks to its very high melting point, is ideal to be used as a heat dissipater without the risk of compromising its physical properties. Therefore, applying a potential difference to the tungsten heads produces a current that is able to heat the crucible due to the Joule effect, transferring to the BaF_2 powder the heat necessary to make it evaporate and disperse in the chamber. Based on the temperature of the BaF_2, it is therefore possible to regulate its vapour pressure within the vacuum chamber. Near the crucible there is an ion production area where the BaF_2 molecules are ionized through collisions with accelerated electrons between an anode and a cathode. The circuit diagram is represented in figure 3.3.

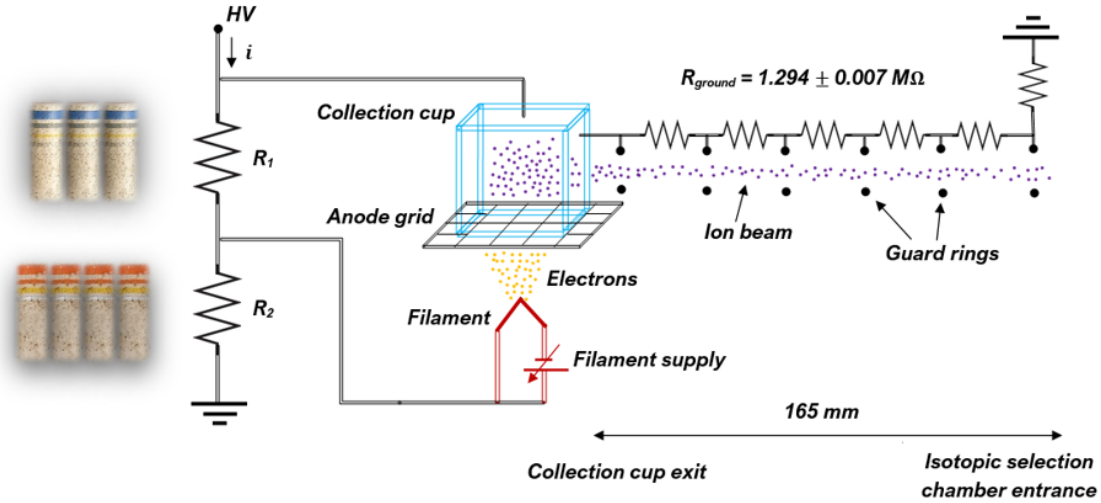

Figure 3.3: Diagram of the circuit. To the left, the images of the resistors of $2.2\, W$ each, with which the last measures were taken: R_1 consisting of 3 equal resistors in parallel, R_2 of 4 resistors in parallel. The circuit is shown in its configuration before the changes to the filament, which was put directly into the collection cup.

The electrons are produced by a filament supplied by a voltage generator (generally a few volts) and are therefore accelerated towards the anode, consisting of a grid placed in front of a collection cup which lies at the same power supply potential (HV). The potential difference between filament and grid is obtained by means of a voltage divider. The collisions between electrons and molecules take place in the space between anode and cathode, thereby creating BaF^+ ions which are collected in the cup. Completing the description of the first stage, the operation of RGA is now explained. This is a mass spectrometer that is widely used in the low pressure gas analysis, consisting of 3 main blocks:

an ionizer, quadrupole rods and a detector. The molecules of the various species in the chamber, once ionized, travel the space between the quadrupole rods that contains a constant electric field overlapped to another one that oscillates at a frequency f. Only ions with a certain mass/charge ratio follow a stable path and pass through the filter. By progressively varying the frequency of oscillation, the RGA is able to measure the ionic current for each atomic mass value, returning the corresponding partial pressure value.

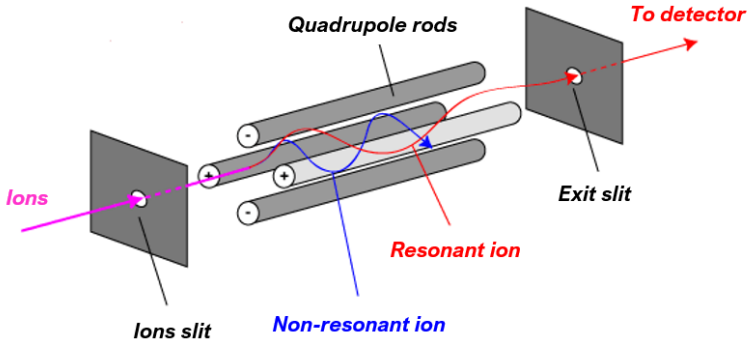

Figure 3.4: RGA scheme

3.2.2 Isotopic selection

For the purposes of the experiment, it is appropriate to obtain ions which are identical to each other, that is, it is necessary to eliminate all the undesirable isotopes of BaF^+. Therefore, the isotope selection starts with the purpose of isolating the most abundant isotope of BaF^+, namely the one with mass $157\,amu$. Note that the isotopic differences are dictated exclusively by barium as fluorine is found in nature in the form of a single isotope at 100%. The ions collected in the cup are then accelerated to ground potential by progressive voltage drops generated by resistors in series, at the ends of which are located guard rings. The beam accelerated in this way is ready to enter the isotopic selection chamber. Due to a number of difficulties in production of the radicals (see paragraph 3.3), in order to be able to take measurements, the BaF_2 was temporarily replaced with Xenon, which is contained in a tank visible in figure 3.1 and enters the production chamber via a leakage valve.

Regarding this second stage of the experiment, a number of studies were undertaken in order to identify the best technique to obtain a distinction of the various isotopes. There are three main possibilities for the type of mass filter that can be used:

a) Magnetic sector mass analyzer

It consists of the classic mass spectrometer with only magnetic field that is able to deflect the ions with a differing radius of curvature depending on their mass. This option was discarded as with the instruments available to us, the magnetic field necessary to deflect the ions is too high. It can be already seen that it is advisable to work with HV that is not overly high in order to obtain more accessible values of B:

$$B = \frac{m\,v}{q\,R} = \frac{m}{q\,R}\sqrt{\frac{2\,\epsilon}{m}} \sim 2\,T \qquad with\ R = 4\,cm,\ \ \epsilon = 2\,keV,\ \ m = 157\,amu \tag{3.2.1}$$

b) Quadrupole mass analyzer

It consists of a dynamic spectrometer that is almost the same as the one used by the RGA: only the ions with a certain mass/charge ratio follow a stable path and pass through the filter. In particular the following results are obtained, inserting the numeric values that can be obtained with the instruments available to us:

$$V = \frac{m\, r^2\, f^2}{0.14} \sim 1.1\, kV \qquad with\ \ r = 2\, cm,\ \ f = 0.5\, MHz,\ \ m = 157\, amu \tag{3.2.2}$$

$$\frac{\Delta m}{m} = \frac{q\, V}{m\, f^2\, L^2} \sim 3\% \qquad with\ \ L = 0.3\, m \tag{3.2.3}$$

The values of the various magnitudes can be obtained without too much difficulty but the problem lies in the resolution in mass, which is still somewhat scarce. In order to try to improve it, it would be necessary to increase as much as possible L. However the length of $30\, cm$ is already quite higher and there would be the risk of excessive divergence of the ionic beam over a similar distance.

c) Wien filter

This system consists of an electric E and a magnetic B field, both constant and orthogonal to each other. It is a speed filter: only ions with a given speed, equal to $v = \frac{E}{B}$ are able to pass undeflected through the filter. As the energy is the same for all the isotopes, a speed difference corresponds to a mass difference. Having defined V as the difference of potential between the electrodes, d their distance and w the opening of the slit upstream of the filter, we obtain the following:

$$B = 10^6 \frac{V}{d\, v} = 10^6 \frac{V}{d} \sqrt{\frac{m}{2\epsilon}} \sim 0.17\, T \qquad V = 350\, V,\ \ d = 4\, cm,\ \ \epsilon = 2\, keV \tag{3.2.4}$$

$$\frac{\Delta m}{m} = \frac{2\, d\, \epsilon\, w}{q\, V\, L^2} \sim 2.8\,\% \qquad w = 0.3\, cm,\ \ L = 22\, cm \tag{3.2.5}$$

Therefore it is possible to obtain a B field that is much lower than that calculated in the first case, with a better resolution and lower length than the quadrupole mass analyzer. This method is therefore more convenient. To create the filter, two permanent magnets are available whose profile, measured by means of a Hall sensor, is shown in figure 3.5. As the magnetic field marked in green is more intense but very variable, with the assistance of magnet experts, it was possible to simulate the corrections to be made in order to uniform it as much as possible (though with a decrease in intensity). Although the magnetic field of the more powerful uniformed magnet is approximately 3 times greater than the other, the choice for the construction of the Wien filter focused on the second one for the following reasons: it is possible to increase the intensity up to 1700 Gauss by reducing the distance between the iron magnets, the initial gradient can be further reduced with the use of foils in such a way as to vary the B field from 0 to the maximum value within $2\, cm$. With these measures, thanks to the fact that the length of the magnet is the most determining parameter for the resolution of the filter, we obtain a resolution as in 3.2.5., that is approximately twice as better than the other magnet. Despite this, it is rather a small value (it would be necessary to come down to at least around 1% using more powerful magnets), also evident from a more precise analysis of deflection of ions (see the next paragraph).

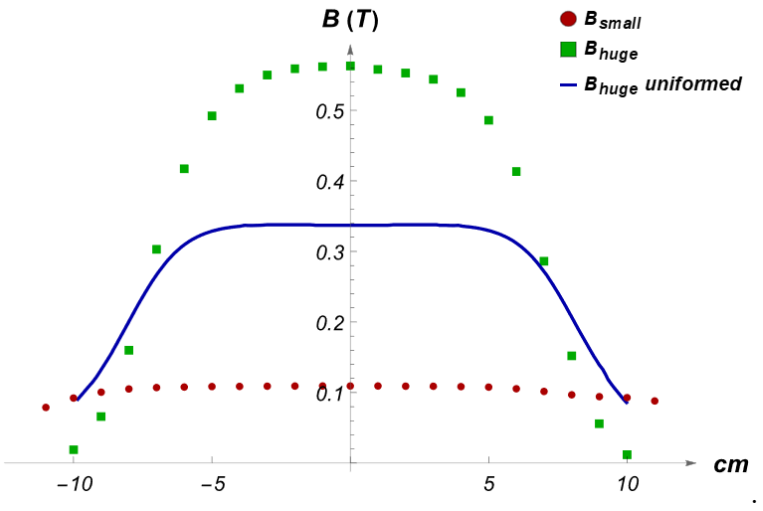

Figure 3.5: Profile of magnetic fields available to us

Due to a number of problems encountered during production of the radicals of BaF^+, it was not possible to set up the magnet and, consequently, there are no measurements on the actual resolving power of the filter. The isotopic selection chamber is currently still empty. Once the magnet is assembled, it will be possible to take measurements to establish the efficacy of the Wien filter.

3.3 Data analysis

A first attempt to observe the production of BaF^+ ions was carried out applying increasing voltage to the electrodes, increasing the current in the tungsten up to $42.0\,A$ corresponding to a voltage of $6.73\,V$, for a total of $283\,W$ dissipated by Joule effect. Analysing the composition of the various molecular species in the chamber via the RGA, a peak near $157\,amu$ is expected, followed by lower peaks due to the barium isotopes. Despite the high intensity of the current, it wasn't possible to view any peak but only a high background, probably due to the products of overheating of the resistors. A subsequent opening of the chamber showed what had been expected, that is depletion of the BaF_2 powder caused by the previous measurements.

It was therefore decided to replace the crucible with a larger one in order to be able to contain a higher quantity of BaF_2. Unfortunately in this situation, a problem in production emerged as, having increased the total mass and the sizes of the crucible, which caused an increase in the thermal capacity which therefore required greater energy to raise temperature. The current in the tungsten was gradually increased up to a maximum of $70\,A$ at $0.91\,V$ of voltage, equivalent to a dissipated power of $64\,W$; it was decided not to further increase the current due to the excessive overheating of the cables in order to avoid melting the sheaths. Unfortunately, no peak greater than the constant base value between $10^{-9}/10^{-10} mbar$, was detected; however it was possible to find an explanation.

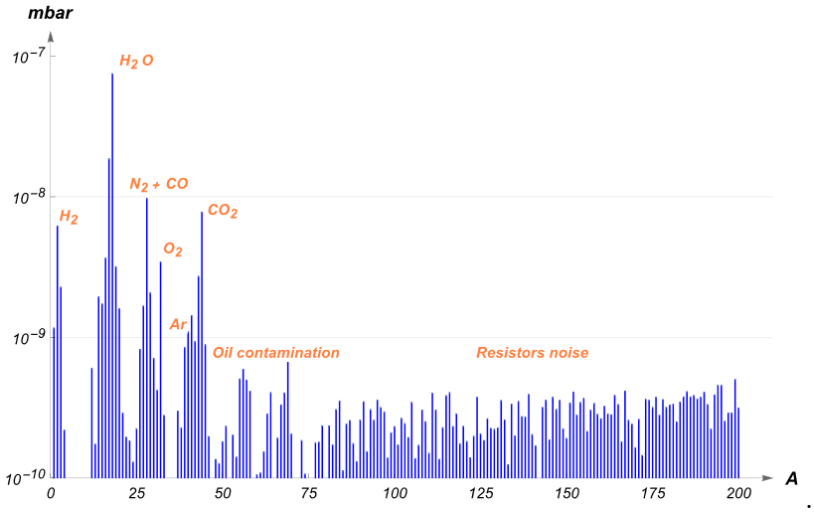

Figure 3.6: Vacuum chamber spectrum. Note the absence of the peak at the BaF^+ mass. The peaks of the various molecular species are recognised as well as the approximately constant base at high mass numbers probably caused by the overheating of the resistors.

In fact, while the tungsten appeared to have a bright orange/yellow colour, the ceramic layer tended to be a dark red while the BaF_2 powder contained in it was almost completely brown. Approximating the system with a black body, it is possible to compare the observed chromatic spectrum with the corresponding temperature. For the brown colour observed in the powder, the maximum possible temperature value is around 900 degrees, after which the colour becomes red. It is therefore possible to compare this temperature with the corresponding partial pressure envisaged for the BaF_2: it involves values that are so low that they don't even fall within the graphic representation (Figure 3.7). However, extending the linear dependence also to the temperatures that we are interested in,

a partial pressure of approximately $6 \cdot 10^{-10}\, mbar$ is obtained, which is consistent with what was observed experimentally. It is therefore necessary to conclude that the method of producing BaF_2 molecules within the chamber is inefficient.

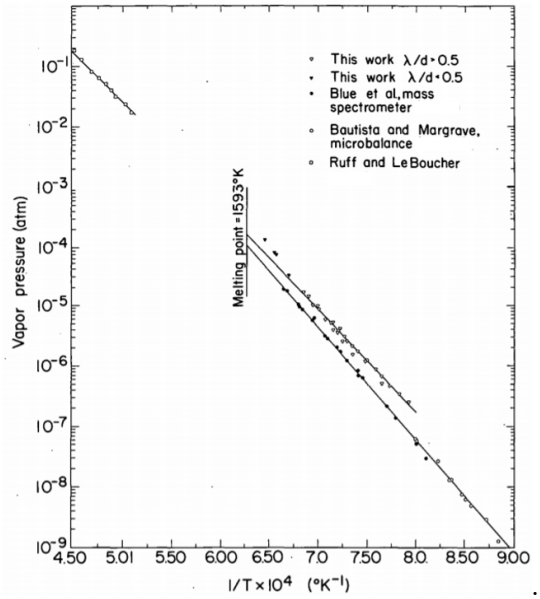

Figure 3.7: Image from [3]: dependance of vapour pressure on temperature for BaF_2 (various experiments).

So, in order to test the extraction of the ionic beam, in the absence of the BaF_2, it was decided to use an element which could be more easily managed and with atomic mass that is fairly similar: Xenon. The chamber was connected to a xenon tank via a leakage valve, used to precisely regulate the pressure inside the chamber. Furthermore, to promote the water desorption (which was particularly difficult to remove due to its high interaction energy with the surfaces of the chamber, approximately $22/24\, kJ/mol$), a nitrogen cylinder was also inserted: creating a layer on the surfaces of the chamber, nitrogen prevents the water from attaching, thereby facilitating its removal.

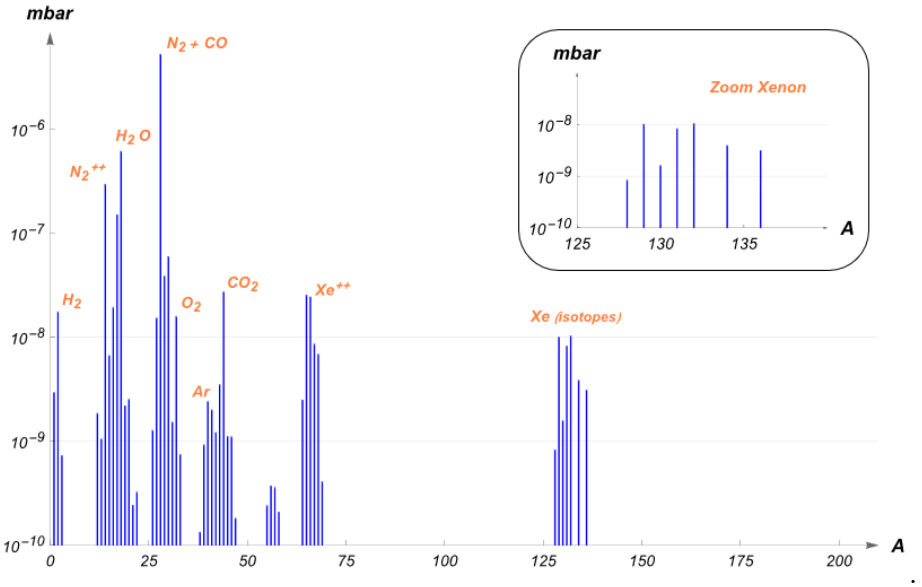

Figure 3.8: Apart from the species shown in the graph, noteworthy are the small peaks at 16 and 17 amu, always caused by the ionized water in the forms HO^+ e O^+, the peaks at 19 and 20 *amu* due to the isotope ^{18}O of the oxygen and finally the peaks at 41, 43 and around the mass 57 due to the backflow of oil, typical of vacuum pumps. Small peaks are due to the rare isotopes of the various elements.

To test the actual concentration of the xenon and that of the parasite components, the spectra were again acquired via the RGA (Figure 3.8), adjusting the pressure inside the chamber to around $10^{-5} mbar$ via the leakage valve (actually, this value read on the analogue pressure gauge was slightly overestimated). As in the previous case, it is possible to see, first and foremost, the various peaks due to the main components of a vacuum chamber, mainly caused by 7 different species. It is observed how the presence of the nitrogen tank significantly raises the peak at $28\,amu$, which would normally be at a lower level than water. Furthermore, the peak at $14\,amu$ is very clear, caused by the nitrogen that is doubly ionized as it enters the RGA and is therefore read as if it had mass 14 (remember that the RGA effectively measures the mass/charge ratio, that corresponds to the mass only regarding the monovalent ions). The same situation is found with xenon, which being, in part, doubly ionised as Xe^{++}, forms various peaks around mass 65. Finally, the various xenon isotopes around mass 130 are clearly visible, which are analysed below. To stabilise the total pressure, all the partial pressures of the individual components of the spectrum are added together. After this, it is possible to obtain the total fraction of the xenon by adding together the contributions of the various isotopes and of the Xe^{++}. Finally, it is possible to calculate the partial pressure of monovalent Xe which will be useful for recognition of the individual isotopes.

total pressure	**Xe fraction**	**Xe^{+} partial pressure**
$\sim 6.56 \cdot 10^{-6} mbar$	$\sim 1.60\%$	$\sim 3.76 \cdot 10^{-8} mbar$

Note the absence of relevant noise components around the atomic masses of the Xe isotopes. There is therefore no risk that in the subsequent stage of the experiment, in which the xenon isotopes are isolated, there could be contaminations of other species with similar atomic mass. It is possible to verify if the RGA is able to recognise with precision the large presence of the various isotopes. In the table, the theoretical expectations are compared with the experimental data, obtained by making the ratio of the partial pressure corresponding to each isotope with the total pressure of Xe in the chamber (this analysis only considers the *monovalent* Xe peaks):

A	**128**	**129**	**130**	**131**	**132**	**134**	**136**
$\%_{th}$	1.91	26.40	4.07	21.23	26.91	10.44	8.86
$\%_{sper}$	2.21±0.26	26.69±0.32	4.21±0.26	21.91±0.30	27.55±0.32	10.32±0.27	8.35±0.27
λ	1.1	0.9	0.5	2.3	2.0	0.4	1.9

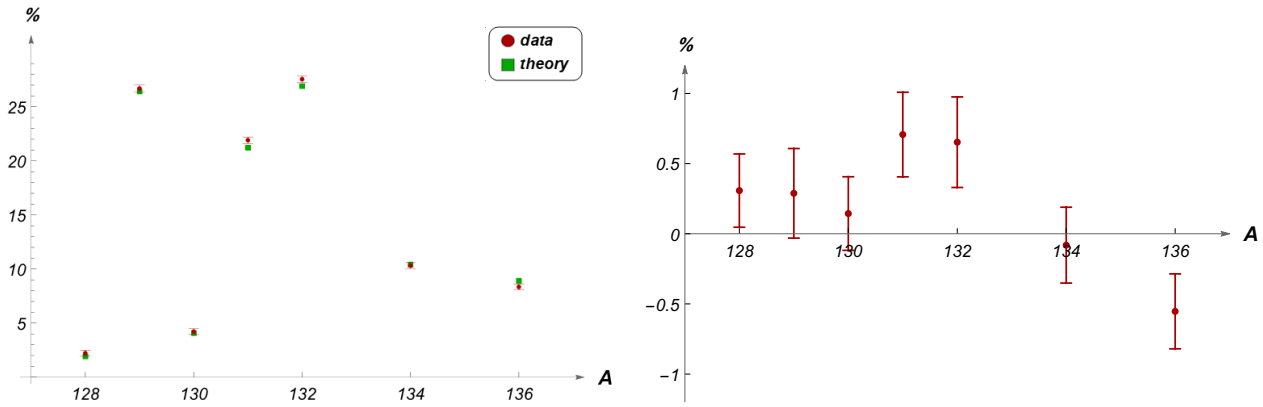

Figure 3.9: To the left, the comparison between the experimental data of percentages and the theoretical expectations. To the right, the residual analysis.

For the errors analysis, a high vacuum spectrum without xenon was measured, considering the background between 50 and 150 *amu* where most of the molecular species are absent. Taking an

average of the height of the various bins, it is possible to estimate with greater precision the background noise. This value constitutes the error associated with the partial pressure for each bin. Therefore the final error on the percentage is obtained through simple propagation:

$$\sigma_{\%} = 100 \sqrt{\left(\frac{1}{p_{Xe,tot}}\right)^2 \sigma^2_{Xe,i} + \left(\frac{p_{Xe,i}}{p^2_{Xe,tot}}\right)^2 \sigma^2_{Xe,tot}} \tag{3.3.1}$$

$$with \;\; \sigma_{Xe,i} = 9.65 \cdot 10^{-11}\, mbar, \;\; \sigma_{Xe,tot} = \sqrt{7\,\sigma^2_{Xe,i}} = 2.55 \cdot 10^{-10}\, mbar$$

Having characterised the spectrum of the atomic and molecular species in the chamber, it was possible to take some measurements for the extraction of the ionic beam. The aim of this was to obtain ionic currents of the order of tens/hundreds of μA to have a sufficient statistic for the final measurements. With the parameters described in the table, the current still didn't go over $12\,nA$ measured at the output from the chamber ($165\,mm$ away from the collection cup), with visible fluctuations in the order of the nA (filament at $3\,cm$ from the grid):

p	**HV**	**filament voltage**	**divider current**	**I_{ion} 165mm**
$10^{-5} mbar$	$2kV$	$1.65V$	$10mA$	$(12 \pm 1)nA$

Therefore the extracted current was much less than was hoped for. The probable reason should be sought in the loss of ions in the $3\,cm$ gap between the filament and the grid: most of the ions produced do not seem to be able to reach the cup and are drawn outwards to ground potential, dispersing in the chamber. As a consequence, the filament was moved into the cup to minimise the loss of ions. Besides this expedient, a picoamperometer was used to measure the ionic current at the entry of the magnet (that will be inserted at a later time for the mass filter) after $325\,mm$ from the beam production point. Clearly, a decrease of the ionic current is expected due to the dispersion of the beam. To try to obtain as much ion current as possible, the divider input current and the filament voltage were further increased. The results obtained are as follows:

p	**HV**	**filament voltage**	**divider current**	**I_{ion} 165mm**	**I_{ion} 325mm**
$10^{-5} mbar$	$2kV$	$2.00V$	$(37 \pm 1)mA$	$\sim 500nA$	$(5.9 \pm 0.3)nA$

First and foremost a significant improvement in the intensity of the extracted current is noted, which, however, is very unstable and still somewhat scarce. Furthermore, the loss of current as a function of distance is quite considerable. Unfortunately, the data collection had to be stopped abruptly as the 2 resistors in parallel that composed R_2 in the divider started to overheat. It was therefore necessary to replace them with more suitable resistors that would be able to withstand a power of up to 2.2W. In particular, R_1 was constructed as the parallel of 3 approximately equal resistors for a total of $R_1 = 271.2 \pm 1.4\,k\Omega$, while R_2 as the parallel of 4 resistors for a total $R_2 = 100.7 \pm 0.5\,k\Omega$. Despite this expedient, also in this case the resistors R_2 overheated with an input current value similar to the previous one. This fact is problematic since the quantity of extracted ions is not yet completely satisfactory and it would therefore be necessary to further increase the input current of the circuit to obtain greater ionization. Unfortunately, with the resistors and the circuit structure used this does not seem possible. So an effort was made to understand the cause of the high power developed on the R_2 resistors to identify a solution.

By analysing the circuit it was understood that the gap between the collection cup and the filament, that is the ionization zone of the xenon atoms, actually constitutes a variable resistance depending on the quantity of ionised atoms. This resistance is placed in parallel with R_1. However, considering that the gas inside the cup is at least partially ionized, it can be assumed that the value of R_1 is on average much greater than that of the variable resistance, thereby promoting the passage of current

through the latter. This justifies the fact that the R_1 resistors have not suffered any kind of damage. On the contrary, the current flowing in R_2 can estimated as being approximately[1]:

$$i_2 = i - i_{ground} = (35 \pm 1)mA \tag{3.3.2}$$
$$where \quad i_{ground} = \frac{HV}{R_{ground}} = (1.55 \pm 0.08)mA, \qquad i = (37 \pm 1)mA$$

As the 4 resistors of R_2 each admit a maximum power of $2.2\,W$, it is possible to obtain the maximum current permitted through each of them. Multiplying by 4 gives the maximum total current on R_2:

$$i_{max} = \sqrt{\frac{P}{R_i}} \sim 2.3mA \implies i_{2,max} = 4i_{max} \sim 9.2mA \qquad (R_i \sim 400k\Omega) \tag{3.3.3}$$

Therefore the maximum current is much lower than what actually flows, which explains why the resistors overheated. Furthermore, this analysis highlights how the potential difference between anode and cathode, which in principle was thought to be adjusted as desired according to the value of HV, is actually sensitive to the quantity of ionized atoms and is therefore not completely controllable. Given the difficulties in the production phase of the BaF_2 molecules, the data collected are limited to the spectra of the components present in the vacuum chamber and to the measurements of the ionic beam extraction efficiency presented above. For the isotopic selection stage it was not possible to proceed beyond the design. In this regard, the result of the calculation of the trajectory of the ion beam through the Wien filter designed in the previous section is shown below. A constant length of $20\,cm$ with an initial and final gradient of $a = 2\,cm$ was considered, assuming that the electric field along y acts only in the constant B section. The following differential equations were solved in the different spatial sections by imposing the boundary conditions for each of them, and the field $e = 10\,060\,\frac{V}{m}$ was regulated in order to let the isotope 132 of xenon (the most abundant) pass non-deflected.

$$\begin{cases} m\,x''(t) &= q\,y'(t)\frac{B_{max}}{a}\,(x(t)+12) \\ m\,y''(t) &= -q\,x'(t)\frac{B_{max}}{a}\,(x(t)+12) \\ -12 \le x \le -10 \end{cases}$$

$$\begin{cases} m\,x''(t) &= q\,y'(t)B_{max} \\ m\,y''(t) &= -q\,x'(t)\,B_{max} + q\,e \\ -10 \le x \le 10 \end{cases}$$

$$\begin{cases} m\,x''(t) &= q\,y'(t)\frac{B_{max}}{a}(12 - x(t)) \\ m\,y''(t) &= -q\,x'(t)\,\frac{B_{max}}{a}(12 - x(t)) \\ 10 \le x \le 12 \end{cases}$$

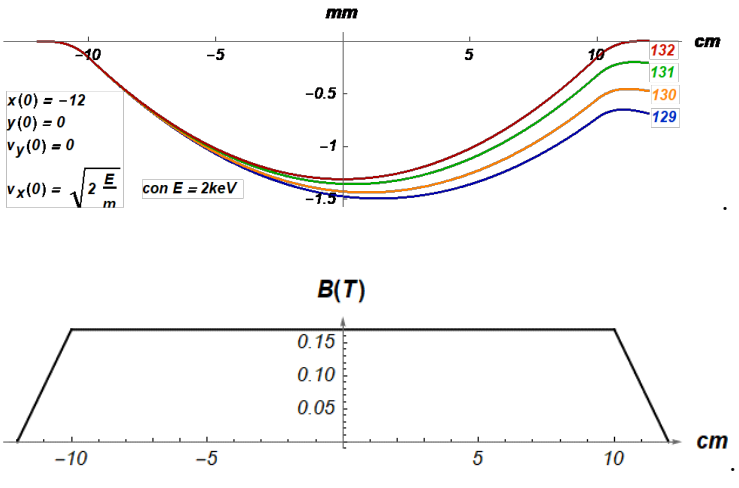

Figure 3.10: Above the trajectories envisaged for the various isotopes, below the profile adopted for the magnetic field.

The expected deflections are at most in the order of $1\,mm$ at the point of exit of the magnetic field therefore, considering the final distance of the matrix (maximum $30\,cm$), slightly greater deflections for the more distant isotopes are achieved. However, the transversal dimension envisaged for the matrix is a few mm in order to obtain a sufficient ion statistic to be studied. Therefore part of the isotopes are not deflected sufficiently and fall within the transverse dimensions of the matrix. In particular, in the case of BaF^+ the situation is more critical as the two most abundant isotopes have paired atomic masses (156 and 157) therefore their distinction would be more complicated.

[1]The errors associated with the quantities stem from an estimate of the fluctuations observed during the measurements, which exceed the sensitivity of the instruments

Conclusions

From the measurements taken on the first stage of the apparatus, a number of clear problems were revealed in the production of BaF^+, starting from the evaporation of the BaF_2 powder. It is therefore advisable to review the production technique. One possibility is the construction of a small oven that can withstand temperatures of up to approximately 1500°C in order to reach a high vapour pressure, enclosing the molecules in a smaller volume than the current one where ionization takes place.

The intensity of the extracted ionic current is still scarce, even if the choice to bring the tungsten filament inside the production cup was right and permitted a significant improvement in the intensity of the ion beam, limiting the loss of ions towards ground potential. It should be noted that it was not possible to raise the input current greatly due to the melting of the resistors. In this regard, it is possible to evaluate a number of modifications to the circuit. Firstly, by inverting the (3.3.3), it is possible to predict the minimum power value that the resistors must withstand in order to avoid damages. This is a value of approximately $30\,W$ which, with a view to increase the input current, can be increased up to around $50\,W$. Resistors with these characteristics can be easily found on the market. Furthermore, by appropriately decreasing the value of R_2 it would be possible to increase the maximum value of permissible current for a certain fixed power. Clearly R_2 cannot be overly decreased as the potential difference between cup and filament would become too high, with the marked risk of sparks.

Furthermore, once the measurements on the resolution permitted by the Wien filter have been taken, it will be possible to determine any corrections. The predictions on the trajectories of the various isotopes, however, leave many uncertainties in this regard and it may be necessary to identify a different and more suitable magnet than the one currently being used.

Finally, the analysis of the spectra reveals a good compatibility between the isotopic percentages observed experimentally and those expected, confirming the correct operation of the RGA as well as the absence of relevant noise components for atomic masses close to those of Xenon and BaF^+. Water is confirmed as the most abundant and difficult to eliminate species.

This new technique for measuring of the electron electric dipole moment is very promising as an improvement of approximately 2 orders of magnitude could reveal the presence of BSM physics. The problems encountered in the initial phases all seem to be resolvable and the greatest difficulty will probably concern the isotope selection stage. Experiments similar to this have considerable importance within the scope of physics today as they are able to investigate new frontiers of physics at undoubtedly low costs, although a very high level of precision is required. Currently, therefore, we are still far from the complete performing of the experimental setup but, thanks also to the collaboration and work of American research groups, it will be possible in the near future to make important progress to further improve, perhaps definitively, the limit of the eEDM.

Bibliography

[1] Barone V., *L'ordine del mondo. Le simmetrie in fisica da Aristotele a Higgs.*, Bollati-Boringhieri, 2013.

[2] Cairncross W.B., Ye J., *Atoms and molecules in the search for time-reversal symmetry violation.*, Nat Rev Phys **1**, pp.510–521, 2019.

[3] Hart P.E., *Vapor pressure and heat of sublimation of barium fluoride.*, California Univ., Berkeley.

[4] Semertzidis Y.K., *Electric Dipole Moments of Fundamental Particles.*, Nucl.Phys.Proc.Suppl.131: 244-251, 2004.

[5] Sakharov A.D., *Violation of CP Invariance, C Asymmetry, and Baryon Asymmetry of the Universe.*, Journal of Experimental and Theoretical Physics Letters, Vol. 5, p.24, 1967.

[6] Semertzidis Y.K., *Review of EDM experiments.*, J. Phys.: Conf. Ser. **335**, 012012, 2011.

[7] Abel C. et al., *Measurement of the Permanent Electric Dipole Moment of the Neutron.*, Phys. Rev. Lett. **124**, 081803, February 2020.

[8] Shapiro F.L., *Electric dipole moments of elementary particles.*, Sov. Phys. Usp. **9**, 345, 1968.

[9] Bennett G.W. et al., *Improved limit on the muon electric dipole moment.*, Phys. Rev. D **80**, 052008, September 2009.

[10] Schiff L.I., *Measurability of Nuclear Electric Dipole Moments.*, Phys. Rev. **132**, 2194, Dec 1963.

[11] Graner B. et al., *Reduced Limit on the Permanent Electric Dipole Moment of* ^{199}*Hg.*, Phys. Rev. Lett. **116**, 161601, January 2016.

[12] Sandars P.G.H., *The electric dipole moment of an atom.*, Phys. Lett. **14**, February 1965.

[13] Abdullah K. et al., *New experimental limit on the electron electric dipole moment.*, Phys. Rev. Lett. **65**, 2347, August 1990.

[14] ACME Collaboration, *Improved limit on the electric dipole moment of the electron.*, Nature **65**, pp.355-360, October 2018.

[15] Khriplovich I.B., Lamoreaux S.K., *CP Violation Without Strangeness. Electric Dipole Moments of Particles, Atoms, and Molecules.*, Berlin, Springer, 1997.

[16] Hudson J.J. et al., *Improved measurement of the shape of the electron.*, Nature **473**, May 2011.

[17] Kozlov M.G., Derevianko A., *Proposal for a Sensitive Search for the Electric Dipole Moment of the Electron with Matrix-Isolated Radicals.*, Phys. Rev. Lett. **97**, 063001, August 2006.

[18] Kirch K., Wellenburg P.S., *Search for electric dipole moments.*, EPJ Web Conf. **234**, 01007, 2020.

[19] Vutha A.C. et al., *Suitability for electron electric dipole moment searches.* Phys. Rev. Lett. **114**, 183001, May 2015.